Tellus (1979), *31*, 13–27

Calculations of free atmospheric shortwave spectral characteristics over the desert (from the CAENEX-70 data)

By K. YA. KONDRATYEV,[1,2] R. M. WELCH,[3] O. B. VASILYEV,[1] V. F. ZHVALEV,[2] L. S. IVLEV[1] and V. F. RADIONOV,[1] [1]*Leningrad State University, Leningrad, U.S.S.R.*, [2]*Main Geophysical Observatory, Leningrad, U.S.S.R.*, [3]*University of Utah, Salt Lake City, Utah, U.S.A., present affiliation Colorado State University, Fort Collins, Colorado, U.S.A.*

(Manuscript received December 22, 1976; in final form August 30, 1978)

ABSTRACT

This report presents a summary of a joint Soviet/American exchange program to compare calculations with observations in the real atmosphere, in order to determine and study the diabatic processes that are important for tropospheric energetics. The primary purpose of the present investigation was to determine the effect of aerosols upon radiation characteristics in the real atmosphere. Spectral measurements of the radiation field as a function of height have been made in 0.01 μm increments from 0.4 μm to 0.9 μm along with aerosol optical properties. Using these data, radiative transfer calculations have been performed using the 4-term expansion of the spherical harmonics method in order to provide an independent check on the accuracy of the previous measurements as well as provide recommendations for improved observations.

The effect of a small amount of highly absorbing material, such as hematite, has been demonstrated. Extensive data are presented giving spectral shortwave radiation flux and flux divergence values as a function of height in the atmosphere. Because no "best fit" overall spectral regions were obtained, further studies were performed to test the sensitivity of the theoretical results to small variations in the input parameters. The results indicate that the major reason for discrepancies between measured and calculated radiation fields is difficulties with the radiative and aerosol measurements, rather than shortcomings of the calculational scheme.

1. Introduction

Extensive experimental investigations have been carried out in recent years as part of the complete Atmospheric Energetics Experiment (CAENEX) program. The data have been obtained from simultaneous surface, airborne, and satellite measurements of the shortwave radiation field for various geographical locations and atmospheric conditions.

Detailed analysis of the experimental results can be performed only on the basis of numerical modelling of radiative transfer under measured atmospheric conditions. In order to properly simulate the radiation field observations, it is necessary to use a theoretical model capable of calculating radiative fluxes to approximately 1% accuracy.

The present work is the result of combined efforts of Soviet and American specialists brought together through an exchange program between the U.S. National Science Foundation and the U.S.S.R. Hydrometeorological Service. The goals of this exchange program are (a) to calculate spectral radiative fluxes, net fluxes and flux divergences in the cloud-free atmosphere from measured optical atmospheric and surface parameters for one of the observational days of the CAENEX program, 25 October 1970, and (b) to compare measured fluxes and flux divergences with calculated results. While further and much more extensive intercomparisons are continuing, the purpose of the present paper is to discuss preliminary results along with the specification of the calculational scheme and optical parameters used in this study.

0040-2826/79/010013-15$02.50/0

2. Experimental data

2.1. *Observational results for spectral fluxes, net fluxes, and divergences of radiative energy on 25 October 1970*

The experiments carried out within the framework of the CAENEX-70 program are thoroughly described in the literature (Kondratyev, 1972, 1973a, b, c, 1975; Kondratyev and Ter-Markaryants, 1976). They were performed over the Kara Kum desert in the vicinity of Repetek, U.S.S.R. The data obtained on 25 October 1970, were taken immediately after a major dust storm and are representative of extremely turbid conditions.

The following observations were made on board the flying laboratory IL-18 of the Main Geophysical Observatory, Leningrad:

(1) Up- and downward flux spectral density by means of a K-2 diffraction spectrometer (spectral range 0.4–0.9 μm, resolution of 0.02 μm, and registering time of 10 s) at altitudes ranging from 300 to 8400 m.
(2) Aerosol number density and size distribution by means of a continuously operating impactor measured on the ground and on the IL-18 aircraft.
(3) Sampling of aerosol matter for further chemical analysis in the surface layer by means of a filter.

The measured data for the up- and downward fluxes were statistically processed so that smoothed spectral characteristics resulted. Statistical processing is necessary in order to compensate for aircraft pitch-and-roll as well as for horizontal variations in aerosol concentrations. These curves are given in 100 mb intervals (interpolating between measured values ranging between 350 and 950 mb, and extrapolating values outside of this range) in graphical form by Kondratyev (1972, 1973b). They are also used for intercomparisons with calculational results and are given in a later portion of this report.

The aerosol particle number density and size distribution for two levels in the atmosphere are given in Table 1.

As a result of spectral analysis of the surface aerosol samples the presence of various elements in the aerosol matter was determined (Table 2).

It should be pointed out that Table 2 does not include the only elements in the aerosol samples. In addition, electron microscopy of the same aerosol samples revealed that together with large, evenly mixed particles described in Table 2, separate spherical compact particles were observed. On the basis of chemical analysis and the photographic image character of these samples, these particles were identified as ferric oxides. Of the metals found in the aerosol samples, only Fe has the atomic weight and concentration large enough to produce the observed frequency

Table 1. *Particle size distribution (μm) of tropospheric aerosol*

		% of aerosol in various size distribution intervals				
Height	Concentration N (cm^{-3})	$r < 0.25\ \mu$m	0.25–0.30	0.30–0.60	0.60–1.20	$r > 1.20\ \mu$m
0	200	0.70	0.14	0.08	0.045	0.035
5500	0.5	0.62	0.19	0.18	0.009	0.002

Table 2. *Contents of various elements (μg/m^3) in the measured aerosol*

	Si	Ca	Fe	Mg	Al	Ni	Cr	Pb	Mn	Cu
Average	13.5	7.2	5.0	2.8	0.9	0.35	0.3	0.3	0.05	0
Minimum content	12.0	6.5	3.0	0.7	0.5	0.3	0.2	0.2	0.03	0
Maximum content	15.0	7.8	7.0	5.0	1.2	0.4	0.4	0.4	0.07	0

of such dense spheres and the deep blackening in the images. However, the impossibility of separating these particles from the principal aerosol mass made it impossible to measure the size distribution for such particles. It was only determined that these spheres are practically of uniform size with an average radius of 0.1 μm. The observations carried out immediately following a severe dust storm suggest that the chemical composition of the aerosol particles was uniform throughout the region of measurement.

2.2. *Optical model of the atmosphere*

On the basis of experimental data and analysis, as well as various literature sources (Hanel, 1972; Kondratyev, 1972, 1973b, c, d), an aerosol optical model was constructed representing the dust loading during the measurement period. This model incorporated the following assumptions: (1) all of the particles are spherical; (2) the particulate index of refraction is spectrally uniform; and (3) the chemical compounds are evenly mixed within each particle as well as throughout particle ensembles. In desert aerosols coated, two-layer particles are essentially not encountered. The assumption of even mixing of all chemical components is reasonable for the fine aerosol fraction but poor for the coarse aerosol fraction. Nevertheless, it is at present not practical to provide detailed calculations of highly complicated multi-component systems. Due to the fact that information concerning dispersion, concentration and index of refraction would be required for each individual particle, a number of simplifications were necessary. The real part of the complex index of refraction for the majority of aerosol components varies from 1.5 to 1.7 in the visible part of the spectrum. Therefore, the scattering characteristics of the coarse aerosol fraction are primarily determined by the particle size distribution rather than by variation of the value of the real part of the refractive index. Furthermore, a mean value of refractive index is justified for the fine aerosol fraction due to strong mixing of the chemical components. Variations of chemical composition observed during this experiment lead to variations in the mean value of the real part of the refractive index of no more than 0.05.

In terms of aerosol model, optical aerosol characteristics are more sensitive to the imaginary part of the refractive index than to the real part. Due to the assumption of uniform chemical composition, errors in aerosol optical characteristics increase with the value of the imaginary part of the refractive index. The component of desert aerosol most differing in value in the complex index of refraction during these measurements was Fe_2O_3 (hematite). For this reason, and because of the almost uniform size of these particles, this aerosol component was treated separately.

The elemental composition of aerosol matter given in Table 2 closely corresponds to the relative component composition of metal-containing compounds in the Ivlev and Popova (1973) model. For this reason, as well as the model assumptions stated above, the Ivlev–Popova model was judged adequate to represent the aerosol optical properties. Applying this model the complex index of refraction for the 0.4–0.9 μm wavelength region was taken to be 1.65–0.005i. It is realized that the value of the complex index of refraction is wavelength dependent. However, such refinements were not included in these preliminary results.

As can be seen from Table 1, rather restricted experimental data on aerosol particle dispersion and concentration were used. In order to calculate attenuation coefficients, along with the scattering phase function, the particle size distribution was extrapolated over the 0.03–10 μm range. In addition, it was assumed that the aerosol optical characteristics vary linearly with pressure within the 1000 to 500 mb layer and were constant with height above this layer. A more complete and detailed aerosol model was not constructed due to the complexities of a more advanced model as well as a lack of complete experimental data from which to produce a more realistic representation. The present work represents a pioneering effort of making detailed intercomparison studies of the atmosphere under extremely turbid conditions. It was one of the objectives of the intercomparison studies to define more closely the accuracy required in measurements and to identify those areas where improvements are necessary.

Values of the absorption, scattering and extinction coefficients as a function of wavelength are given in Table 3 for the surface and at a height of 5500 m. From the data of Table 3 it is seen that the absorption, scattering, and extinction

coefficients normalized by particle number increase with height. This is a result of the fact that the particle size distribution function varies with height. At high altitudes there is an increase in the percentage of optically more active particles. This phenomenon is related to coagulation of small particles and fallout of the large particles at great heights where particle residence times are larger than in the lower atmospheric layers.

The effect of the previously described aerosol model is primarily to scatter solar radiation. Note that absorption is usually less than 15% of extinction in Table 3. However, there is a maximum observed "residual" aerosol absorption which is not accounted for the present aerosol model in the wavelength region 0.40–0.50 μm. Presumably the strong aerosol absorption observed in this region was contributed by hematite, Fe_2O_3, which was included separately.

Coefficients of absorption, scattering, and extinction due to hematite particles, not included in the previously described aerosol distribution, were calculated for a number of models. Since the hematite particles had an extremely narrow size distribution with radii of approximately 0.1 μm, a delta-function size distribution was constructed initially. However, due to oscillations in the Mie efficiency curves, small variations in particle size may lead to large variations in attenuation parameters. Therefore, a number of hypothetical narrow size distributions were constructed with the following properties (with corresponding attenuation coefficients given in Table 4):

A:	N =	111	222	333	222	111		Particles/cm^3
	r =	.08	.09	.10	.11	.12		μm
B:	N =	111	222	333	222	111		Particles/cm^3
	r =	.01	.05	.1	.15	.2		μm
C:	N =	111	222	333	222	111		Particles/cm^3
	r =	.10	.11	.12	.13	.14		μm
D:	N =	50	100	200	300	200	100	50 Particles/cm^3
	r =	.04	.06	.08	.1	.12	.14	.16 μm

Table 3. *Absorption, scattering and extinction coefficients (in km^{-1} for $N = 10^3$ particles/cm^3) as a function of wavelength at $H = 0$ m and 5500 m for the observed size distribution of aerosol particles*

	H = 0 m			H = 5500 m		
λ (μm)	β_{abs}	β_{scat}	β_{ext}	β_{abs}	β_{scat}	β_{ext}
0.40	0.38	2.42	2.80	0.55	3.80	4.35
0.45	0.32	2.44	2.76	0.60	3.65	4.25
0.50	0.29	2.49	2.78	0.65	3.50	4.15
0.60	0.26	2.49	2.75	0.62	3.30	3.66
0.70	0.25	2.44	2.69	0.40	3.26	3.66
0.80	0.24	2.39	2.63	0.35	3.00	3.35
0.90	0.23	2.44	2.57	0.36	2.84	3.20

In contrast to the highly variable Mie calculations for monodisperse aerosol, the attenuation coefficients in Table 4 for the various size distributions are surprisingly similar. Model A considers a narrow size distribution centered about particle radius $r = 0.1$ μm, while model B considers a much broader distribution also centered about $r = 0.1$ μm. Extinction coefficients are quite similar for these two models. However, absorption coefficients are considerably larger for model B than for model A, particularly for the larger wavelengths. Model D, which has a size distribution intermediate between models A and B, also has attenuation coefficients intermediate in value between those of models A and B. The extinction coefficients for models A, B and D are roughly similar, indicating that the Mie values are

Table 4. *Absorption (β_a) and extinction (β_e) coefficients for hematite (in km^{-1} for $N = 10^3$ cm^{-3}) as a function of wavelength (λ) for several size distribution models (see text)*

	Model A		Model B		Model C		Model D	
$\lambda(\mu m)$	β_a	β_e	β_a	β_e	β_a	β_e	β_a	β_e
0.40	3.52 – 2	1.00 – 1	3.38 – 2	1.04 – 1	5.07 – 2	1.10 – 1	3.42 – 2	9.71 – 2
0.45	2.24 – 2	1.22 – 1	3.01 – 2	1.30 – 1	3.34 – 2	1.18 – 1	2.55 – 2	1.14 – 1
0.50	8.56 – 3	1.44 – 1	1.84 – 2	1.30 – 1	1.39 – 2	1.39 – 1	9.72 – 3	1.23 – 1
0.55	6.32 – 3	1.60 – 1	1.56 – 2	1.44 – 1	1.19 – 2	1.71 – 1	9.06 – 3	1.21 – 1
0.60	5.59 – 3	1.62 – 1	1.03 – 2	1.21 – 1	9.54 – 3	2.14 – 1	7.23 – 3	1.45 – 1
0.65	4.71 – 3	1.57 – 1	1.49 – 2	1.70 – 1	5.16 – 3	2.31 – 1	4.72 – 3	1.44 – 1
0.70	2.83 – 3	1.29 – 1	5.37 – 3	1.36 – 1	3.94 – 3	2.49 – 1	3.51 – 3	1.34 – 1
0.75	1.63 – 3	8.89 – 2	1.90 – 3	1.25 – 1	3.76 – 3	2.51 – 1	2.04 – 3	1.34 – 1
0.80	1.24 – 3	5.20 – 2	2.06 – 3	1.09 – 1	4.69 – 3	2.13 – 1	1.99 – 3	1.04 – 1
0.85	7.02 – 4	3.10 – 2	4.19 – 3	1.38 – 1	4.25 – 3	1.65 – 1	1.79 – 3	8.99 – 2
0.90	3.96 – 4	2.10 – 2	4.67 – 3	1.74 – 1	2.61 – 3	1.13 – 1	1.69 – 3	8.45 – 2

Table 5. *Vertical distribution of Fe_2O_3 particle concentration*

H (km)	0	1	2	3	4	5	6	7	8
N (cm^{-3})	1000	800	500	300	250	200	100	50	25

particularly sensitive to the peak or center of the distribution rather than the width of the distribution. However, the absorption coefficient appears to be more sensitive to the width or the large particles in the distribution. Model C considers the same distribution as model A, but with the center of the distribution shifted to $r = .12$ μm. Even this small shift leads to significantly larger attenuation parameters, particularly at the larger wavelengths. The results in Table 4 show that much more accurate measurements of size distribution are required. Due to the variability of these results an ambiguity exists which cannot be resolved within the framework of the present measurements. Model D was chosen as the "standard" hematite model used in the intercomparison studies. However, results were obtained with each of the other models and compared.

It should be noted that due to the strong variation of Mie efficiency factors with small variations in size parameter, a small increment in size parameter ($\Delta X \sim .1$) is required to eliminate errors from calculations involving polydispersions. The hematite models A, B, C and D have been calculated with a larger increment of size parameter. However, more detailed sample calculations with a finer increment do not substantially change these values nor the interrelationships between the models. Due to the fact that these models only represent hypothetical situations, with the lack of direct measurements of the hematite size spectrum, and for the sake of economy, more detailed calculations were not performed.

The vertical distribution of Fe_2O_3 particle concentration is given in Table 5. This particle concentration profile was calculated based upon data concerning the profile of mass concentration of Fe_2O_3 in the total aerosol assuming an average hematite particle radius of $r = .1$ μm.

Due to a lack of data on vertical profiles of water vapour and oxygen, gaseous absorption was neglected in the present investigation. Only absorption by ozone in the Chappuis band was accounted for. Since only total ozone content was measured, the vertical profile was obtained from mean latitudinal vertical distributions (Kondratyev and Vasilyev, 1975; Vasilyev and Fedorov, 1975).

Molecular scattering was taken into account according to Etterman's model (Kondratyev, 1969).

3. Calculation of radiation characteristics of the atmosphere

3.1. *Method of spherical harmonics*

The calculation method follows the spherical harmonics approach as developed by Zdunkowski and Korb (1974). This technique has been applied to cloud models by Welch et al. (1976) and to polluted urban atmospheres by Welch and Zdunkowski (1976), and has been extended to include the infrared window by Korb et al. (1975). However, an extension of this model has been used in the present calculations.

In the delta-Eddington model developed by Joseph et al. (1976), the peak of the scattering phase function is replaced by a delta function. This technique has been shown to provide significantly more accurate values of radiative fluxes. Wiscombe (1977) has extended this approach for higher order terms and Welch and Cox (1978) have applied this approach to the spherical harmonics technique. Comparison of the delta-spherical harmonics and adding techniques for clouds (Welch and Cox, 1978) shows that this approach provides accurate values of both radiative fluxes as well as flux divergences. The reader is referred to the literature for details of the calculation procedure.

The vertically inhomogeneous atmosphere was divided into ten horizontally homogeneous layers. Optical properties were assumed constant within each of these vertical layers, and fluxes and mean intensities are continuous at each interface.

The atmosphere is horizontally inhomogeneous and the observations have been statistically averaged at each observational height to provide the horizontally homogeneous average values necessary for the computational procedure. The present theoretical calculations, likewise, represent the average radiative flux values at a given height in the atmosphere. When very detailed horizontal measurements become available, horizontally inhomogeneous radiation calculations using a technique comparable to the Monte Carlo method would be desirable. At present, however, shortwave flux measurements require 10 s to sweep through the spectral range 0.4–0.9 μm during which the aircraft will have encountered various horizontal inhomogeneities. Furthermore, it is not possible for the aircraft to follow the identically same track at various altitudes. In addition the solar zenith angle changes during the course of the observations. Therefore, the present theoretical procedure assuming an averaged horizontally homogeneous atmosphere appears to be a reasonable compromise for these preliminary calculations.

4. Comparison between the calculated and experimental data

4.1. *Comparison between the calculated and measured radiation characteristics of the free atmosphere for three models*

Fig. 1 shows both calculated (solid lines) and measured (dashed lines) values of the upward ($F\uparrow$) and downward ($F\downarrow$) fluxes at four levels within the atmosphere. $F\downarrow$ refers to the combination of direct and diffuse components of the radiative flux. Label 1 refers to the uppermost level of measurement (8400 m) and label 4 refers to the lowest level of measurement (300 m); label 2 refers to a height of 3000 m while label 3 refers to a height of 1300 m. Both aerosol and hematite (Model D) are included in the calculations. Input data for the calculations consist of $F\downarrow$ at level 1; therefore, the solid and dashed lines at level 1 are constrained to be identical for plots of $F\downarrow$. There is reasonable agreement in the values of $F\downarrow$ except near the surface, indicating that the aerosol concentration in the lower layer is too large. However, the discrepancies in $F\uparrow$ between calculated and measured values are large. Calculated values of the upward flux are significantly larger than measured values. Fig. 1 also shows calculated and measured values of the net flux ($F_N = F\downarrow - F\uparrow$) and spectral heating rates ($\partial\theta/\partial t$). Computed values of F_N and ($\partial\theta/\partial t$) also show large disagreement with measured values. It should be noted that values of the spectral heating rate are particularly sensitive to accurate measurements of upward and downward fluxes, heating rates being calculated from net flux divergences. The wild fluctuation of measured values of heating rates may be attributed to

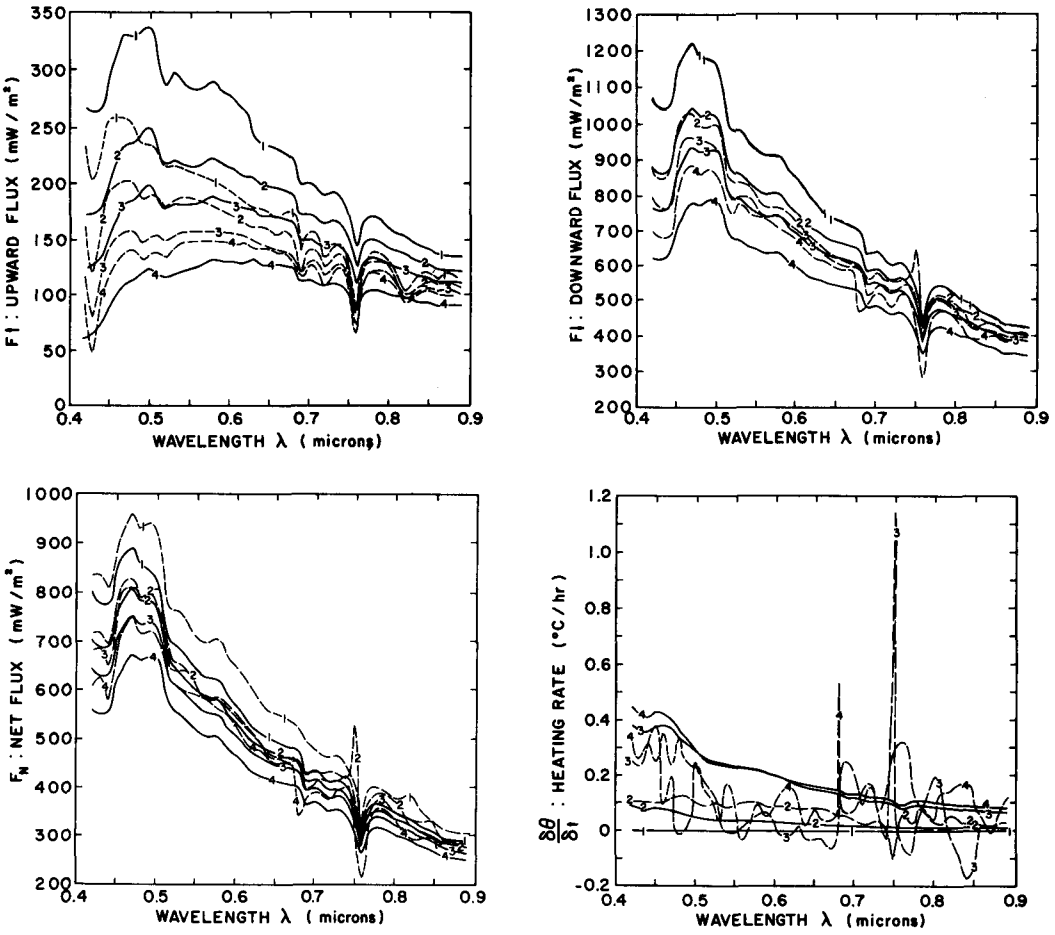

Fig. 1. Values of the upward ($F\uparrow$), downward ($F\downarrow$) and net (F_N) fluxes (in MW/m^2) along with heating rates ($\partial\theta/\partial t$ in °C/h) as a function of wavelength (in μm). Calculated values are given by solid lines and measured values are given by dashed lines. Labels 1–4 refer to altitudes of 8400, 3000, 1300 and 300 m, respectively. This model includes aerosol, hematite (model D), Rayleigh scattering and gaseous absorption.

horizontal inhomogeneities in aerosol concentration, pitch and roll of the aircraft, and the fact that the same flight path is not followed exactly at the various vertical levels.

The purpose of this paper is to analyze these discrepancies shown in Fig. 1 more thoroughly and to offer possible reasons for such discrepancies with the idea of improving the accuracy of future measurement programs.

One possible cause of such discrepancies between measured and calculated values is the accuracy of the calculational scheme. The original calculations were made using the four-term expansion of the spherical harmonics technique. However, all of the solutions presented in this report have utilized the delta-spherical harmonics technique. Detailed calculations using these data have shown only small differences using these two calculational approaches. As a further check detailed calculations using the adding method (Wiscombe, 1976) substantiate the accuracy of the present approach. Therefore, it is safe to assume that no theoretical errors or calculational instabilities are responsible for the discrepancies shown in Fig. 1.

One is led to the conclusion that there are some errors either in the measurement of fluxes or in the aerosol analysis. Measurements were

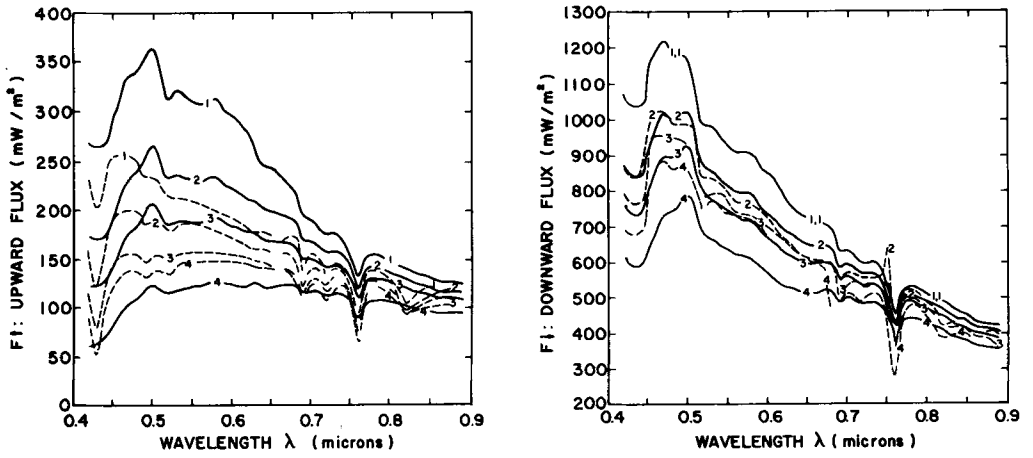

Fig. 2. Same as in Fig. 1 except only upward and downward fluxes are given. This model substitutes the hematite $r = .10$ μm delta function for hematite model D.

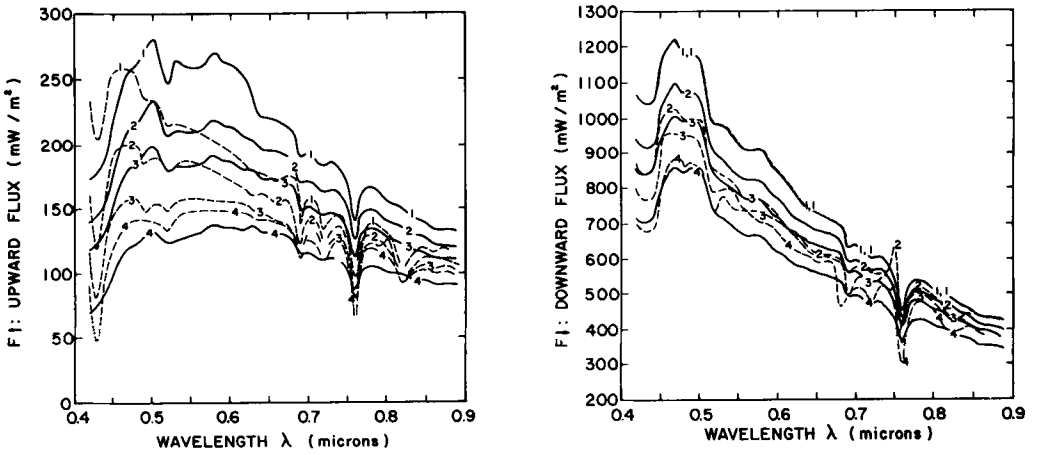

Fig. 3. Same as in Fig. 1 except only upward and downward fluxes are given. Rayleigh scattering has been neglected.

taken with a mean solar zenith angle of 54°, however, during the measurement process the solar zenith angle was changing. Calculations using solar zenith angles ranging from 50° to 58° show that such variations lead to flux differences of several percent. However, variations of this amount are not sufficient to account for the large discrepancies between calculations and measurements. Calculations also show that 25% errors in the assumed Rayleigh or gaseous absorption parameters likewise lead to only small variations in calculated fluxes.

Another possibility for error exists in the assumed hematite model used in the calculations. Table 4 shows the variation in hematite attenuation parameters for various delta function and size distribution models. All of these various models were run, but with only small variations in fluxes. Results obtained using models A, B, C and D were so similar that plots using these models will not be shown here. Variations in the spectral fluxes did not exceed 2% for such models. However, the delta function models did show slightly more variation, with sharper maximum values. Fig. 2 shows $F\uparrow$ and $F\downarrow$ applying the $r = .10$ μm hematite delta function model along

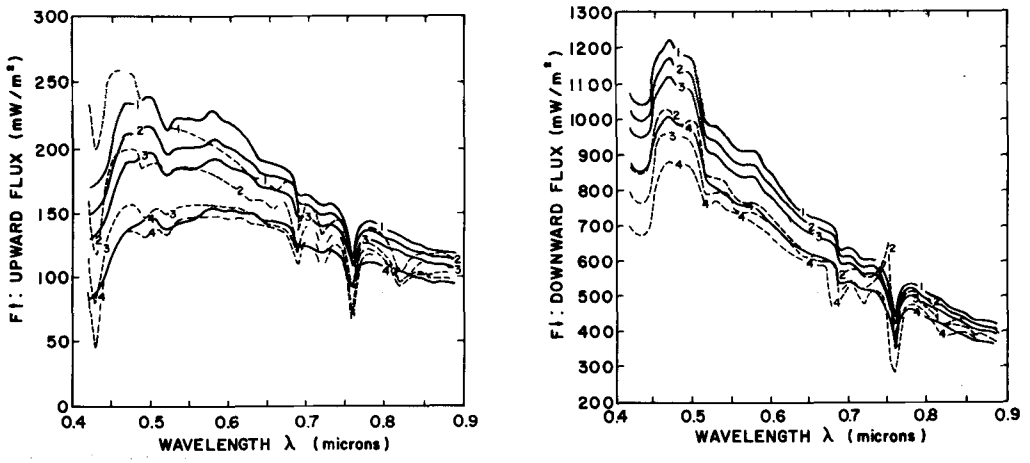

Fig. 4. Same as in Fig. 1 except only upward and downward fluxes are given. Both hematite scattering and absorption and Rayleigh scattering have been neglected.

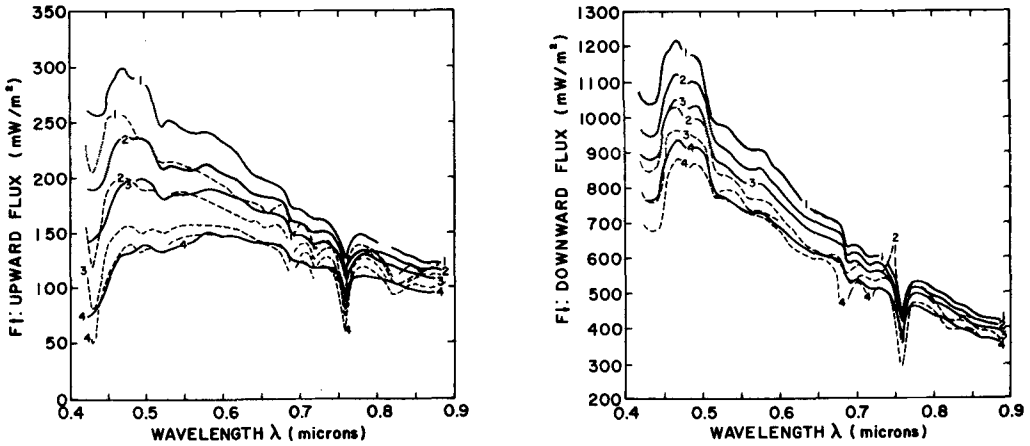

Fig. 5. Same as in Fig. 1 except only upward and downward fluxes are given. Hematite has been deleted from this model.

with the standard aerosol model. Comparison of Figs. 1 and 2 shows that variation of the assumed hematite particle size distribution has only slight influence on the calculated radiative fluxes.

The relative contribution of various components to the radiative fluxes is shown in Figs. 3 and 4. Fig. 3 shows the $F\uparrow$ and $F\downarrow$ spectral fluxes neglecting Rayleigh scattering. Comparison of Figs. 1 and 3 shows that the large peak in upward flux at short wavelengths is due to Rayleigh scattering. Fig. 4 shows the $F\uparrow$ and $F\downarrow$ spectral fluxes neglecting Rayleigh scattering and hematite. Comparison of Figs. 3 and 4 shows the relative contribution due to hematite, while Fig. 4 shows the contribution by the aerosol alone (Table 3). Using the aerosol alone (no hematite or Rayleigh scattering) provides better agreement between the measured and calculated upward fluxes, but leads to large errors in the downward fluxes. For completeness Fig. 5 shows the $F\uparrow$ and $F\downarrow$ spectral fluxes using the aerosol and Rayleigh scattering, but neglecting hematite entirely. Comparison of Figs. 1 and 5 shows the effect of hematite alone. The effect of hematite is to increase the upward spectral fluxes somewhat; the effect on the downward spectral flux shows that hematite

is responsible for about 15% of the total aerosol optical thickness. Neglect of hematite (Fig. 5) shows somewhat better agreement with measurements (than Fig. 1), although with major differences remaining. This set of calculations indicates that an overestimate of hematite concentrations could, in part, be responsible for some of the discrepancies between measurement and calculations, but not all.

Another possibility for error lies within the measurement of the spectral fluxes. The upward-looking spectrometer mounted on the roof of the IL-18 aircraft measures primarily the direct solar beam. However, the downward-looking spectrometer (measuring $F\uparrow$) receives only diffuse flux. It was theorized that perhaps the design of a flat-plate instrument might lead to underestimates of diffuse flux due to reflections at angles larger than the Brewster angle. Such errors would be greatest for isotropic scattering in highly turbid atmospheres. An analysis of the instrumentation indicated that a combination of shielding factors could have reduced the measurement of diffuse flux by a maximum of 25%. Fig. 6 shows the results of increasing the measured values of $F\uparrow$ by 25% using hematite model C. The measured values of surface albedo have also been scaled upward by 25%, since these values were measured from the aircraft. As can be seen from Fig. 6 significantly improved agreement now results between measurements and calculations using this 25% scaling. Similar errors in the upward-looking (measuring $F\downarrow$) instrument may have also been present. At the top of the atmosphere (8400 m) there is essentially no diffuse flux so that the measurements taken here are exact. At low levels in an extremely turbid atmosphere there is an increase in diffuse flux along with a decrease in direct solar flux. Therefore, similar errors in measurement might be expected for the values of $F\downarrow$ at lower levels in the atmosphere. However, such corrections at level 4 for $F\downarrow$ leads to more disagreement between the dashed and solid lines. Of course errors in measurement of diffuse flux would be quite significant in highly turbid atmospheres in which the radiation is nearly isotropic (i.e., clouds in particular). Fig. 6 also shows the spectral net fluxes and spectral heating rates. Heating rates of up to 0.5 °C/h are predicted using this model for wavelengths of <0.45 μm. However, these values appear to be too large. In any case, there appears to be a strong spectral dependence in the heating rates, with maximum values at the shorter wavelengths.

There was one other study completed in which hematite scattering was neglected while including hematite absorption. Such a model assumes that the hematite is embedded in the main aerosol particles and does not exist independently in the atmosphere. Hematite, however, showed up in the sample analysis as independent particles. In order for this model to be valid it must be supposed that the impactor shattered all of the large aerosol particles in order to provide the individual hematite particles, all roughly of the same size, which were observed. Fig. 7 shows the spectral upward, downward and net fluxes along with the spectral heating rates. As shown, this model provides reasonable agreement between calculations and measurements. Heating rates of 0.4 °C/h are predicted at the shorter wavelengths (0.45 μm), decreasing to 0.15 °C/h at the longer wavelengths (0.8 μm). This mechanism provides the most realistic simulation of the measured results.

The previous analyses may be considered as sensitivity studies as well as intercomparison studies. Surface spectral albedo was measured from the aircraft at a height of approximately 300 m. However, due to the turbid atmospheric conditions, these measurements may have been somewhat in error.

As a final sensitivity study the surface albedo was varied to determine the resulting variation in spectral fluxes. However, downward spectral fluxes were only slightly affected by even major variations in surface albedo. Fig. 8a shows upward spectral fluxes with the surface albedo set to zero, while Fig. 8b shows upward spectral fluxes with the value of surface albedo doubled. These large variations in surface albedo were chosen to more clearly illustrate its effect upon the upward spectral fluxes. Measured values of the surface spectral albedo measured at a height of 300 m are given in Table 6. As shown there is a strong increase in the value of surface albedo with increasing wavelength in the 0.4 to 0.9 μm wavelength region.

Fig. 8 shows that even for this highly turbid atmosphere large variations in surface albedo strongly affect the upward diffuse flux at all levels in the atmosphere. At a wavelength of .5 μm $F\uparrow = 335$ mW/m^2 (Fig. 1) at an altitude of

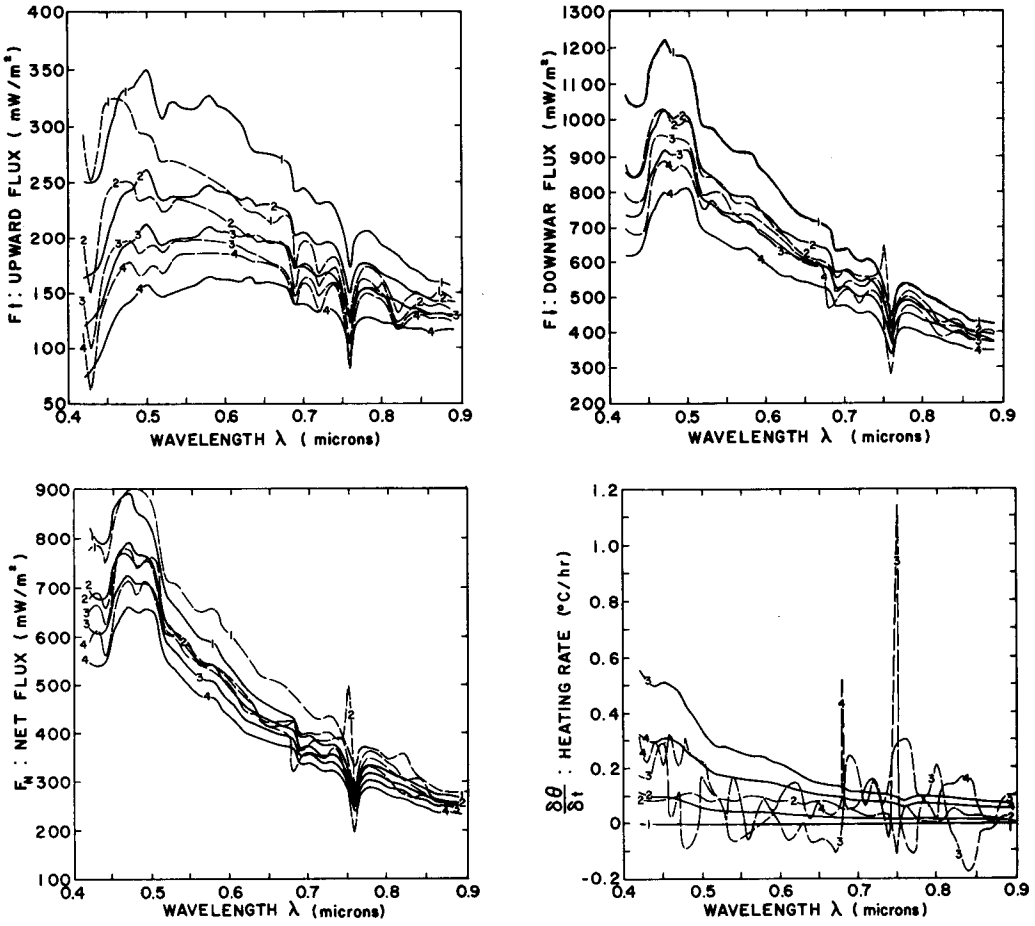

Fig. 6. Same as in Fig. 1. Hematite model C is used and the measured values of $F\uparrow$ have been increased by 25%.

8400 m. Decreasing surface albedo to zero reduces this value to 255 mW/m² (Fig. 8a) while doubling the surface albedo increases this value to 415 mW/m². In this case a variation of 15.3% in surface albedo led to a variation of upward diffuse flux of 80–90 mW/m², or about 5–6 mW/m² per 1% variation in surface albedo. At a wavelength of 0.8 μm $F\uparrow = 160$ mW/m² at an altitude of 8400 m; decreasing surface albedo to zero reduces this value to 85 mW/m² while doubling the surface albedo increases this value to 245 mW/m². In this case a variation in surface albedo of 24.5% led to a variation in upward diffuse flux of 75–85 mW/m² or about 3 mW/m² per 1% variation in surface albedo. These values suggest that variations in surface albedo have a larger impact at the shorter wavelengths.

Values in the upward diffuse flux intermediate between those of Figs. 1 and 8a might be suggested for heavy dust loading over a water surface (albedo of about 5%), while variations in upward diffuse flux suggested in Fig. 8b might be representative of heavy dust loading over a highly reflective surface such as snow. It is realized that the actual surface spectral reflectance over water and snow may be quite different from those values given in Table 6. It is merely suggested that these figures give a qualitative description of the variation of upward diffuse flux over such surfaces.

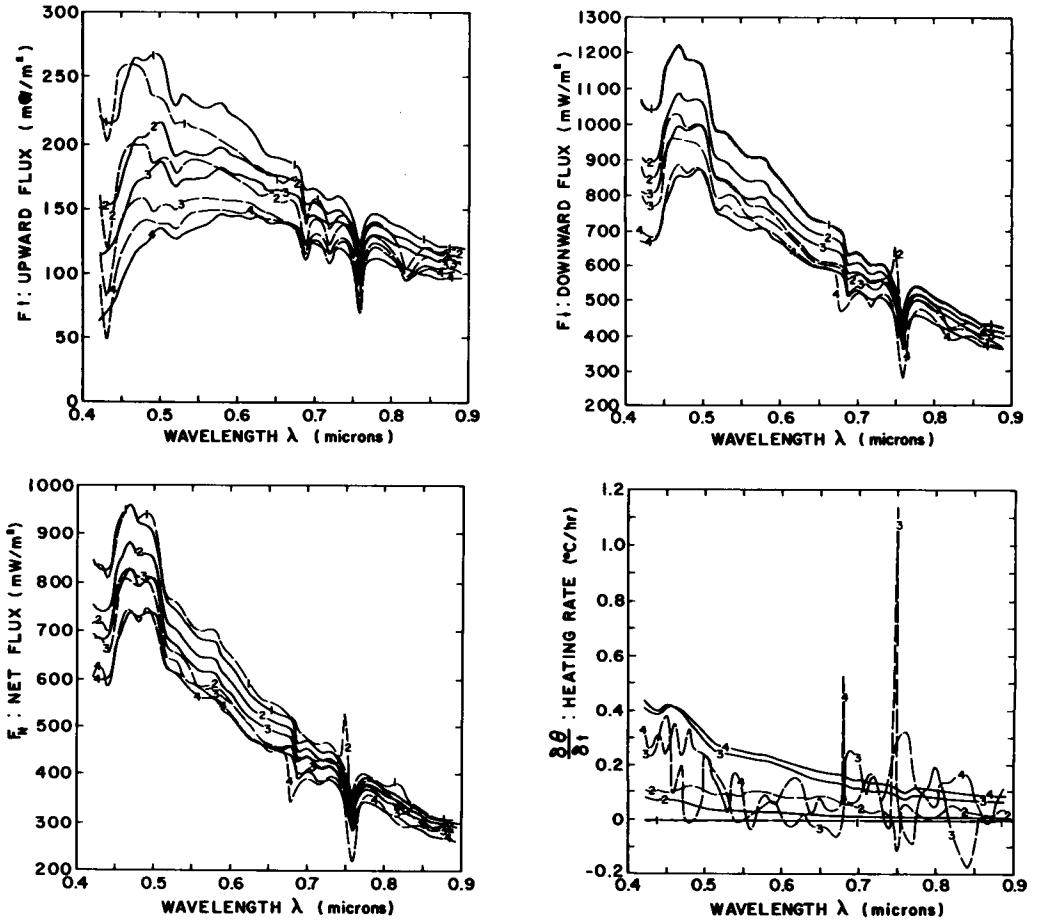

Fig. 7. Same as in Fig. 1. Hematite scattering has been neglected while including hematite absorption.

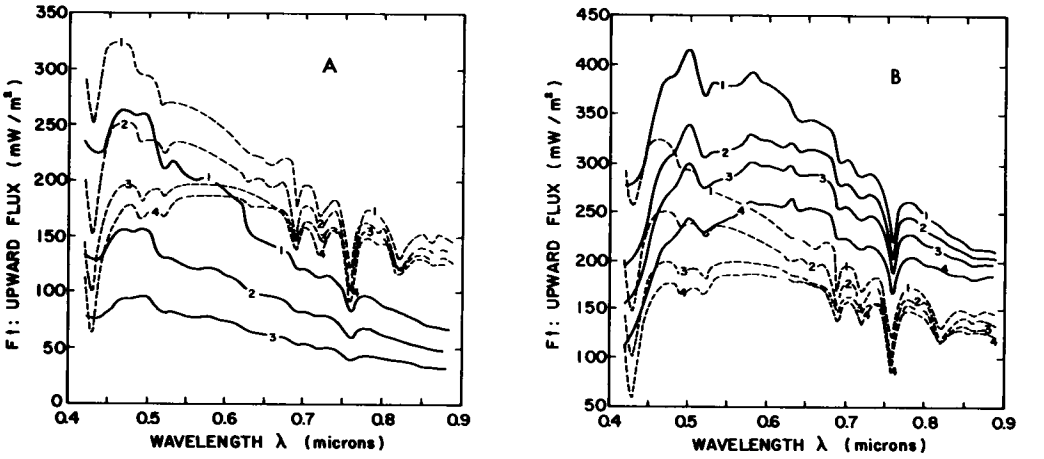

Fig. 8. Same as in Fig. 1 except only upward fluxes are given. (A) is for values of the spectral surface albedo set to zero, while (B) is for the values of the spectral surface albedo doubled.

Table 6. *Surface spectral albedoes* (%) *at selected wavelengths as measured from an altitude of 300 m*

Wavelength (μm)	.42	.47	.52	.57	.62	.67	.72	.77	.82	.87
Surface albedo	9.2	13.6	16.7	20.0	22.5	23.1	23.4	24.3	24.8	26.0

5. Conclusion

The present research indicates how close cooperation between those involved in theoretical modelling and those involved in measurement and analysis of observational data can benefit both sides in providing deeper understanding of those parameters necessary for a complete and accurate description of the earth's radiation budget. In particular, actual data indicate where deficiencies in current models need to be improved as well as supply such models with real data to simulate the real atmosphere. Likewise, comparison of accurate theoretical models with observational data helps those involved in field studies better appreciate which data are critical for proper evaluation of the radiation field and where increased resolution is required.

Due to saturated impactor samples taken under highly turbid conditions, measurements of aerosol concentrations, size distributions, chemical composition and optical properties are unreliable to an unknown degree. Studies concerning the hematite size distribution show that a delta function approximation is not sufficient to model hematite absorption. However, various narrow hematite size distributions provide similar optical properties. In any case, the discrepancies between observed and calculated spectral fluxes cannot be resolved from any variation of the hematite optical properties. Furthermore, reasonable variations of solar zenith angle, Rayleigh scattering parameters and ozone parameters are also too small to correct for the observed discrepancies.

The present analysis was able to indicate two possible mechanisms large enough to account for such discrepancies. The first possibility is that the spectrometers are underestimating the diffuse flux. As discussed, this kind of error would be most serious in the measurement of the upward flux. Increasing the measured upward fluxes by 25% brings the calculations and measurements into rough agreement. There are some indications that the instrumentation may have errors of this magnitude, but until thorough analysis is made, no estimates will be available. The second possibility is that the particle impactor thoroughly pulverized the large aerosol particles. The hematite may have been totally contained within the large particle conglomerate rather than existing as independent particles. In this case, one might reasonably neglect hematite scattering while still including hematite absorption. Such an eventuality also brings the observed and calculated values into rough agreement. In fact, a combination of these two possibilities may be responsible.

The present CAENEX-70 observational program may be viewed as a pioneering effort in this area. At the time of the measurements, these problems were not fully appreciated. The present study indicates in particular that: (1) a much more careful calibration of the spectrometers is necessary, particularly at large angles; (2) the impactor should not be allowed to become saturated, thereby making accurate particle size distribution counts difficult, and (3) there should be some other method of taking particle counts so as to insure that large particle conglomerates are not shattered, thereby giving an improper particle size distribution.

6. Acknowledgements

This research has been supported by the U.S. National Science Foundation and the U.S.S.R. Hydrometeorological Service. Computer calculations were performed at the National Center for Atmospheric Research (NCAR) and at the Main Geophysical Observatory (MGO).

The authors would like to extend their thanks to C. Ridley and B. Chavez on the NCAR staff and to E. Sorokin of the MGO for their efforts to expedite this research effort. Thanks are also extended to P. Martin for proofreading the manuscript, to S. Wunch for typing the manuscript and to J. Owen-Ashbaugh for assistance with the figures.

REFERENCES

Hänel, G. 1972. The ratio of the extinction coefficient to the mass of atmospheric aerosol particles as a function of the relative humidity. *Aerosol Sci. 3*, 455–460.

Ivlev, L. S. and Popova, S. J. 1973. A complex index of refraction for the dispersed phase of atmospheric aerosol. *Izvestia of the U.S.S.R. Ac. Sci. Physics of the Ocean and Atm. 9*, No. 1D.

Joseph, J. H., Wiscombe, W. J. and Weinman, J. A. 1976. The Delta-Eddington approximation for radiative flux transfer. *J. Atmos. Sci. 33*, 2452–2459.

Kondratyev, K. Ya. 1969. Radiative characteristics of the atmosphere and the Earth's surface. Gidrometeorizdat, Leningrad, 564 pp.

Kondratyev, K. Ya., ed. 1972. Complete atmospheric energetics experiment (CAENEX-70 expedition data). *Proceedings of the Main Geophysical Observatory, 276*, Gidrometeorizdat, Leningrad, 279 pp.

Kondratyev, K. Ya., ed. 1973a. Complete atmospheric energetics experiment (CAENEX-71). *Proceedings of the Main Geophysical Observatory, 296*, Gidrometeorizdat, Leningrad, 140 pp.

Kondratyev, K. Ya., ed. 1973b. Complete atmospheric energetics experiment (results of research, 1970–1972). *Proceedings of the Main Geophysical Observatory, 322*, Gidrometeorizdat, Leningrad, 84 pp.

Kondratyev, K. Ya., ed. 1973c. Complete atmospheric energetics experiment (CAENEX). *VNIIGMI—MCD*, Obninok, 79 pp.

Kondratyev, K. Ya., et al. 1973d. Aerosol impact of radiation transfer—possible climatic effects. Leningrad State University Publication, 266 pp.

Kondratyev, K. Ya., ed. 1975. The complete energetics experiment (CAENEX-73). *Proceedings of the Main Geophysical Observatory, 366*, Gidrometeorizdat, Leningrad, 98 pp.

Kondratyev, K. Ya. and Ter-Markaryants, N. E., eds. 1976. Complete radiation experiment. Gidrometeorizdat, Leningrad, 240 pp.

Kondratyev, K. Ya. and Vasilyev, O. B. 1975. Die bedentung des aerosols fur den strahlungshaushalt und sein möglicher eingluss auf das klime. *Zeitschrift fur Meteorologie*, Heft 3, Band 25, pp. 129–142.

Korb, G. J., Welch, R. M. and Zdunkowski, W. G. 1975. An approximative method for the determination of infrared radiative fluxes in scattering and absorbing media. *Contrib. Atmos. Phys. 48*, 85–94.

Vasilyev, O. B. and Fedorov, V. V. 1975. Vertical profiles of free atmosphere spectral optical parameters over the desert. *Problems of Atmospheric Physics*, Vol. 13, pp. 33–75. Leningrad State University Press.

Welch, R. M., Geleyn, J. F., Korb, G. J. and Zdunkowski, W. G. 1976. Radiative transfer of solar radiation in model clouds. *Contrib. Atmos. Phys. 49*, 128–146.

Welch, R. M. and Zdunkowski, W. G. 1976. A radiation model of the polluted atmospheric boundary layer. *J. Atmos. Sci. 33*, 2170–2184.

Welch, R. M. and Cox, S. K. 1978. Absorption of solar radiation in clouds. Part I. The effect of monomodal drop size distributions, cloud top heights, cloud thickness, and vertical water vapor upon cloud heating rates and the cloud radiation field. Submitted *to J. Atmos. Sci.* for publication.

Wiscombe, W. J. 1976. On initialization, error, and flux conservation in the doubling method. *J. Quant. Spectrosc. Radiat. Transfer 16*, 637–658.

Wiscombe, W. J. 1977. The delta-M method: rapid yet accurate radiative flux calculations for strongly asymmetric phase function. *J. Atmos. Sci. 34*, 1408–1422.

Zdunkowski, W. G. and Korb, G. J. 1974. An approximative method for the determination of shortwave radiative fluxes in scattering and absorbing media. *Contrib. Atmos. Phys. 47*, 129–144.

РАСЧЕТЫ КОРОТКОВОЛНОВЫХ СПЕКТРАЛЬНЫХ ХАРАКТЕРИСТИК СВОБОДНОЙ АТМОСФЕРЫ НАД ПУСТЫНЕЙ. (ПО ДАННЫМ КЭНЭКС-70)

Данная статья является итогом совместной советско-американской программы сравнений расчетов с измерениями в реальной атмосфере с целью определения и исследования неадиабатических процессов, существенных для энергетики тропосферы. Главной целью настоящего исследования было изучение влияния аэрозолей на радиационные характеристики реальной атмосферы. Наряду с определением оптических характеристик аэрозоля были проведены спектральные измерения поля радиации в зависимости от высоты в диапазоне от 0,4 до 0,9 мкм с шагом 0,01 мкм. С целью независимой проверки точности вышеупомянутых измерений, а также для выработки рекомендаций по совершенствованию наблюдений с использованием этих данных были выполнены расчеты переноса радиации с применением 4-х членного разложения по методу сферических гармоник.

Был продемонстрирован эффект присутствия незначительных количеств активно поглощающего материала, как, например, гематита. Представлены общирные данные по величинам спектральных потоков и притоков коротковолновой

радиации как функции высоты в атмосфере. Поскольку не было получено наилучшего совпадения во всех спектральных областях, были проведены дальнейшие исследования по оценке чувствительности теоретических результатов к малым изменениям входных параметров. Предварительные результаты указывают на то, что теоретические результаты чувствительны к распределению различных компонентов аэрозоля по размерам.